Cell Reports
Physical Science

CellPress
OPEN ACCESS

Article

Solar Thermoradiative-Photovoltaic Energy Conversion

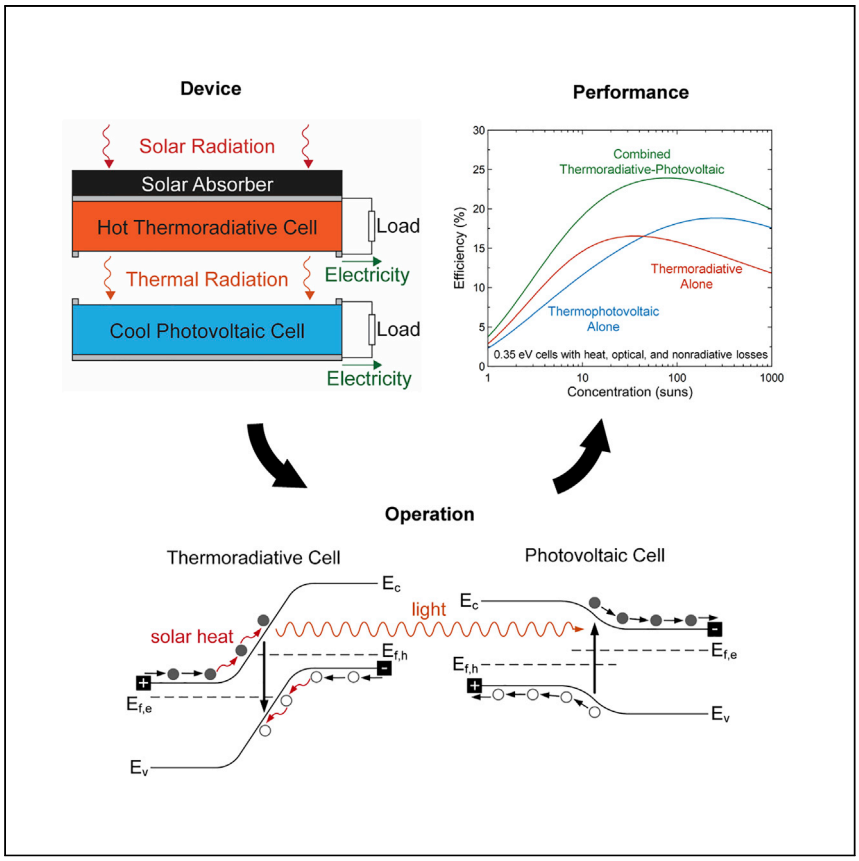

Tervo et al. propose a solid-state heat engine for solar-thermal conversion: a solar thermoradiative-photovoltaic system. The thermoradiative cell is heated and generates electricity as it emits light to the photovoltaic cell. Combining these two devices enables efficient operation at low temperatures, with low band-gap materials, and at low optical concentrations.

Eric J. Tervo, William A. Callahan, Eric S. Toberer, Myles A. Steiner, Andrew J. Ferguson

eric.tervo@nrel.gov

HIGHLIGHTS

A solar thermal converter that uses thermoradiative and photovoltaic cells

Ultimate efficiency limit is 85%, and ideal single-junction one-sun limit is 45%

Low band-gap systems perform well at low optical concentrations

System with losses can outperform comparable solar thermophotovoltaics by ~8%

Tervo et al., Cell Reports Physical Science *1*, 100258
December 23, 2020
https://doi.org/10.1016/j.xcrp.2020.100258

Cell Reports
Physical Science

CellPress
OPEN ACCESS

Article

Solar Thermoradiative-Photovoltaic Energy Conversion

Eric J. Tervo,[1,3,*] William A. Callahan,[1,2] Eric S. Toberer,[1,2] Myles A. Steiner,[1] and Andrew J. Ferguson[1]

SUMMARY

A continuous supply of renewable energy requires intermittent sources to be paired with storage. Thermal storage is an excellent match for solar energy, but concentrating solar power plants must use high optical concentrations and large plants to be cost competitive. Here, we propose an alternative, solid-state heat engine for solar-thermal conversion consisting of a solar absorber, a thermoradiative cell, and a photovoltaic cell. Heat from the solar absorber or thermal storage drives radiative recombination current in the thermoradiative cell, and its emitted light is used by the photovoltaic cell. Based on the principle of detailed balance, we calculate a limiting solar conversion efficiency of 85% for fully concentrated sunlight and 45% for one sun with an absorber and single-junction cells of equal areas. Solar thermoradiative-photovoltaic systems outperform similar solar thermophotovoltaic converters for low band gaps and practical absorber temperatures, and for a realistic device, this improvement can be up to 7.9% (absolute).

INTRODUCTION

To achieve an electricity grid based on renewable generation, intermittent sources including solar energy must be paired with storage. Thermal energy storage is a very attractive solution due to its simplicity, scalability, and low cost,[1–5] especially compared to electrochemical battery storage.[6] However, thermal storage precludes the use of direct solar-to-electricity conversion with photovoltaics (PVs) unless extremely high storage temperatures are used.[7] Instead, sunlight is absorbed as heat and used to immediately or later (with thermal storage) drive a heat engine. Modern concentrating solar power plants accomplish this with thermomechanical cycles that use large turbomachinery, resulting in high capital costs.[8,9] Accordingly, concentrating solar power plants generally must be very large for cost-competitive electricity generation. This has helped to motivate research into alternative, solid-state heat engines that could also offer simplicity, scalability, and low cost.[10–12]

One type of solid-state heat engine that has received significant attention is the thermophotovoltaic (TPV) converter.[13–15] A TPV system consists of a hot emitter of thermal infrared photons that replaces the sun and a PV cell that converts those photons to electricity.[16–18] When the emitter is heated directly or indirectly (via thermal storage) by sunlight, this is a solar TPV system, as illustrated in Figure 1A. Solar TPVs have a very high maximum theoretical solar conversion efficiency of 85% for fully concentrated sunlight on a black absorber.[19] This has motivated a number of theoretical[20–26] and experimental[14,27–31] studies of solar TPVs, but experimental solar conversion efficiencies have only reached 8.4%.[14] High solar TPV efficiencies are difficult to achieve in practice because they favor relatively high band gaps (>0.6 eV) and emitter temperatures (>1,500 K),[11,19,21,32] which also leads to large thermal

[1]National Renewable Energy Laboratory, Golden, CO 80401, USA

[2]Department of Physics, Colorado School of Mines, Golden, CO 80401, USA

[3]Lead Contact

*Correspondence: eric.tervo@nrel.gov

https://doi.org/10.1016/j.xcrp.2020.100258

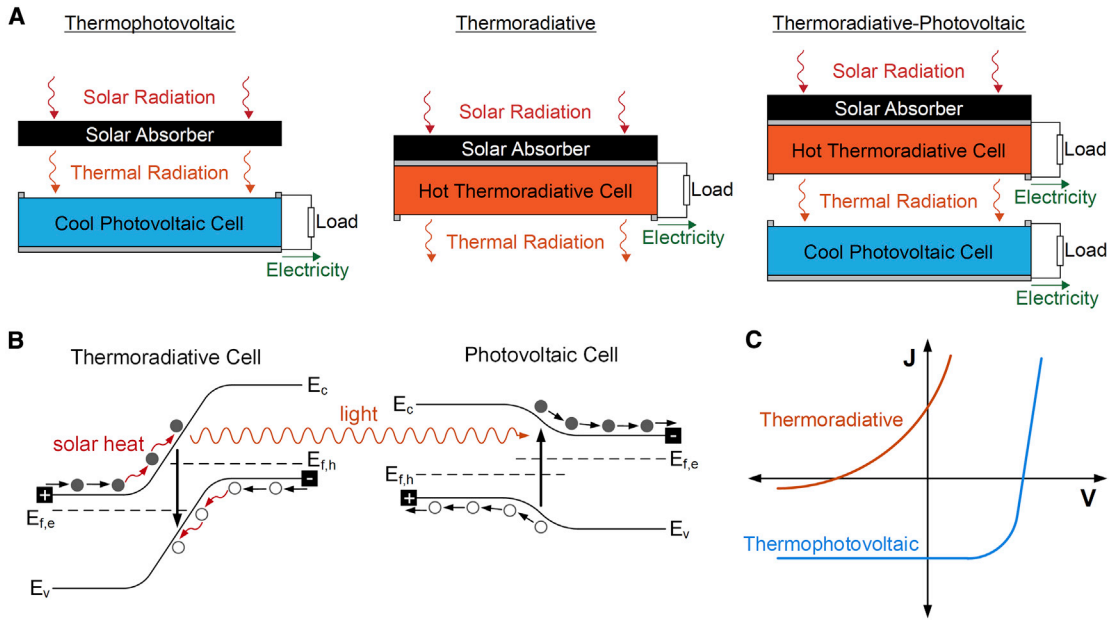

Figure 1. Diagram and Operation of a Solar Thermoradiative-Photovoltaic Conversion System

(A) Schematic of a solar thermophotovoltaic, a solar thermoradiative, and a solar thermoradiative-photovoltaic energy converter.

(B) Band diagrams of the thermoradiative and photovoltaic cells.

(C) Current-voltage diagram of the two devices. A solar thermoradiative-photovoltaic converter produces electricity from both cells simultaneously.

losses. Despite their challenges, TPV systems have a number of beneficial characteristics, such as the ability to modify the photon spectrum and recycle unused photons to the thermal emitter. For example, sub-band-gap parasitic absorption can be drastically reduced by using nanophotonic selective emitters[29,30,33,34] or selectively absorbing cells with a rear mirror.[13,35–37]

A related technology that could operate efficiently with lower band gaps and lower hot-side temperatures is the thermoradiative (TR) cell or negative illumination photodiode.[38,39] TR cells have the same p-n architecture as PV cells, but instead of being illuminated by an external photon source, they are directly heated and allowed to thermally radiate to a colder temperature environment, as illustrated in Figure 1A. The resulting net emission of above-band-gap thermal photons can be thought of as a "negative illumination," causing a nonequilibrium depletion of minority carriers by radiative recombination. This corresponds to a splitting of quasi-Fermi levels and device voltage opposite that of a PV cell under illumination, as shown in Figure 1B. A continuous current is enabled by diffusion of charge carriers toward the junction and a sufficient heat supply for those carriers to overcome the junction voltage, which is also illustrated in Figure 1B. In contrast, PV cells rely primarily on drift (movement of charges due to the built-in electric field) to separate electron-hole pairs and enable a continuous current. As a result, TR cells produce power in the second quadrant of a current-voltage plot, whereas PV cells produce power in the fourth quadrant, which is depicted in Figure 1C. Even though TR cells are a relatively new concept, they have already been demonstrated experimentally[40–42] and have been shown to have great potential as emissive energy harvesters.[43–50] As with solar TPVs, TR converters could be used for solar energy conversion by heating the TR cell with sunlight via a solar absorber or thermal storage.[51] However, solar TR systems favor very low band-gap (<0.3 eV) materials, making them more sensitive to nonradiative losses.[39,51]

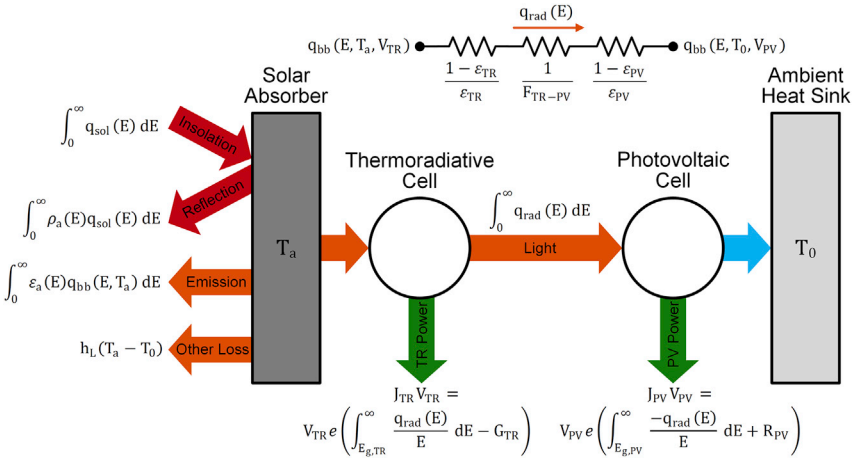

Figure 2. Diagram of Energy Fluxes and Governing Equations for the Solar Thermoradiative-Photovoltaic System

The photovoltaic cell is at temperature T_0 by thermal coupling to the ambient heat sink, and the thermoradiative cell and absorber are at a temperature T_a determined by an energy balance. The spectral radiative heat flux between the cells, q_{rad} (E), is determined with a series of radiative thermal resistances shown above the schematic and is calculated according to Equation 7.

To use the advantages of both TPV and TR systems, it is natural to consider a heated TR cell emitting to a cool PV cell and obtaining power from both devices.[52] In this article, we propose such a system for solar energy conversion: a solar TR-PV converter, as shown in Figure 1. We develop a detailed-balance model of the system and use this model to derive its efficiency limit of 85% under maximum concentration. We then consider a more practical configuration of an ideal one-sun area-matched absorber, TR cell, and PV cell, and we show that its efficiency can reach 45% and exceeds that of a solar TR or solar TPV converter for low to moderate band gaps and absorber temperatures. Finally, we examine a more realistic converter with combined loss mechanisms under optical concentration and demonstrate that it can achieve efficiency gains by up to 7.9% in comparison to solar TPVs under low solar concentration.

RESULTS

Theory

Let us consider a solar TR-PV system with the energy fluxes, as illustrated in Figure 2. A spectral solar radiation flux q_{sol} (E) is incident on the absorber, which may be concentrated or unconcentrated light. For simplicity and clarity when examining performance trends, we model solar radiation as normally incident light from a blackbody at temperature $T = T_s = 6{,}000$ K, which gives similar efficiency results as the use of the AM 1.5 G or concentrated AM 1.5 D spectrum.[53] In this framework, the spectral solar radiation flux is given by[19,54]

$$q_{sol}(E) = \eta_o C_o f_s q_{bb}(E, T_s), \qquad \text{(Equation 1)}$$

where E is the photon energy, η_o is the optical concentration efficiency that we take as unity, C_o is the optical concentration ratio, $f_s = \Omega_s/\pi$ is a geometric factor that accounts for the limited solid angle occupied by the sun, where $\Omega_s = 6.8 \times 10^{-5}$ sr,[19,53,54] and q_{bb} (E,T) is the spectral blackbody emissive power defined as

$$q_{bb}(E, T) = \frac{2\pi}{h^3 c^2} \frac{E^3}{e^{\frac{E}{kT}} - 1} \qquad \text{(Equation 2)}$$

Some of this light will be reflected according to the spectral reflectance $\rho_a(E)$ of the absorber, and the remainder is absorbed assuming that no light is transmitted. Some of the absorbed energy may be lost by the emission of thermal radiation, convection, or conduction. Spectral emission losses are given by $\varepsilon_a(E)\ q_{bb}\ (E,T_a)$, where $\varepsilon_a(E)$ is the spectral emittance of the absorber. For an opaque surface, $\varepsilon_a(E)$ is equal to the spectral absorptance $\alpha_a(E) = 1 - \rho_a(E)$, according to Kirchhoff's law. T_a here is the absorber temperature and the TR temperature. We group convection and conduction losses according to $h_L(T_a - T_0)$, where h_L is the loss coefficient and $T_0 = 300$ K is the ambient temperature and PV temperature. All of the energy not reflected or lost is transferred to the TR cell. In practice, this transfer can be achieved by thermal conduction, with direct contact between the absorber and TR cell, or through intermediate heat exchangers and a heat transfer fluid, as is done in most concentrating solar power plants.[8] With the latter approach, thermal storage may also be integrated into the system in a straightforward manner.

The TR and PV cells can be readily modeled with the detailed balance formalism[39,46,48] common to PV analysis.[54] For the TR cell, emission of a single above-band-gap photon corresponds to a single charge carrier, which may complete a circuit consisting of the TR cell and external load, as illustrated in Figure 1B. Losses in PV cells are recombination losses, which decrease the population of excess minority carriers toward its equilibrium value (Figure 1B). In TR cells with a depletion of minority carriers, however, losses are generation losses that increase the population of minority carriers toward its equilibrium value (Figure 1B). These generation losses include radiative, Auger, Shockley-Read-Hall, and surface processes analogous to those in PV cells,[55] which can impede transport and reduce the negative illumination current. The current density in the TR cell can therefore be described by

$$J_{TR} = e\left[\int_{E_{g,TR}}^{\infty} \frac{q_{rad}(E)}{E}\,dE - G_{TR}\right], \qquad \text{(Equation 3)}$$

where e is the electron charge, $E_{g,TR}$ is the band gap of the TR cell, $q_{rad}(E)$ is the net spectral radiation flux from the TR cell to the PV cell, and G_{TR} is the nonradiative generation rate. Because $q_{rad}(E)$ is a net quantity, radiative generation losses are included in this expression of the current. Similarly, the current density in the PV cell is

$$J_{PV} = e\left[\int_{E_{g,PV}}^{\infty} \frac{-q_{rad}(E)}{E}\,dE + R_{PV}\right], \qquad \text{(Equation 4)}$$

where $E_{g,PV}$ is the band gap of the PV cell and R_{PV} is the nonradiative recombination rate. The values for G_{TR} and R_{PV} are determined according to the framework established by Shockley and Queisser.[54] For both the TR cell and the PV cell, a factor f_c is defined, which represents the radiative fraction of generation/recombination in a p-n diode, such that $f_c = 1$ corresponds to zero nonradiative loss, $f_c = 0.1$ corresponds to 10% radiative and 90% nonradiative generation/recombination, and so forth. Since the radiative generation/recombination rate is embedded in the $q_{rad}(E)$ term, lower values of f_c increase nonradiative losses without changing radiative generation/recombination, and the voltage dependence of $q_{rad}(E)$ is passed on to G_{TR} and R_{PV}. f_c is used to calculate nonradiative loss rates at the ambient temperature T_0 for both devices, because this will provide consistent nonradiative losses in the TR and PV cells and because radiative generation losses in the TR cell result from thermal radiation coming from the PV cell at temperature T_0. Any temperature dependence of the cell band gaps, nonradiative losses, or emittances is neglected.

The net spectral radiative heat flux from the TR cell to the PV cell, $q_{rad}(E)$, in Equations 3 and 4 depends not only on the device temperatures and optical properties but also on their voltages due to luminescence effects. This can be included by modifying the blackbody emissive power as[56,57]

$$q_{bb}(E,T,V) = \frac{2\pi}{h^3c^2}\frac{E^3}{e^{\frac{E-\mu}{kT}}-1}, \quad \text{(Equation 5)}$$

where $\mu = qV$ for $E \geq E_g$ and $\mu = 0$ for $E < E_g$. Because both the TR and PV cells are emitting radiation and may reflect some of that radiation back to the other device, $q_{rad}(E)$ is most easily determined from a radiation resistance network, as shown at the top of Figure 2. The blackbody emissive powers of the TR and PV cells given by Equation 5 are the two boundary nodes in the network, and the three resistances in series between them are the TR surface resistance (which accounts for the optical properties of the TR cell), the space resistance (which accounts for the view factor between the TR and PV cells), and the PV surface resistance (which accounts for the optical properties of the PV cell) defined as[58]

$$R_{surf,TR} = \frac{1-\varepsilon_{TR}(E)}{A_{TR}\varepsilon_{TR}(E)},\ R_{space} = \frac{1}{A_{TR}F_{TR-PV}},\ R_{surf,PV} = \frac{1-\varepsilon_{PV}(E)}{A_{PV}\varepsilon_{PV}(E)}, \quad \text{(Equation 6)}$$

where $\varepsilon_{TR}(E)$ and $\varepsilon_{PV}(E)$ are the spectral emittances of the TR and PV cells, A_{TR} and A_{PV} are their surface areas, and F_{TR-PV} is the view factor of the PV cell from the TR cell. We assume that the cells have equal areas and are spaced very closely in comparison to their lateral dimensions, such that $F_{TR-PV} \approx 1$ and the area terms may be removed to obtain a radiation flux. The net spectral radiative flux from the TR cell to the PV cell is then calculated as

$$q_{rad}(E) = \frac{q_{bb}(E,T_a,V_{TR}) - q_{bb}(E,T_0,V_{PV})}{R_{surf,TR}+R_{space}+R_{surf,PV}} \quad \text{(Equation 7)}$$

The preceding paragraphs fully describe the energy flows in this solar TR-PV system. Once the optical properties (ε_a, ε_{TR}, ε_{PV}, $E_{g,TR}$, $E_{g,PV}$), loss coefficient (h_L), voltages (V_{TR} and V_{PV}), and nonradiative losses (G_{TR} and R_{PV}) are selected, an energy balance on the absorber and TR cell can be solved for T_a. Once T_a is known, it can be used to calculate other performance indicators such as output powers and losses. The solar TR-PV efficiency can then be calculated as

$$\eta = \frac{-A_{TR}J_{TR}V_{TR} - A_{PV}J_{PV}V_{PV}}{A_a\int_0^\infty q_{sol}(E)dE}, \quad \text{(Equation 8)}$$

where A_a is the area of the solar absorber and the negative signs are used because the JV product for both cells is negative. We note that while the discussion thus far has focused on energy flows per unit area, A_a, A_{TR}, and A_{PV} need not be equal. In fact, there may be advantages in having $A_a < A_{TR}$, because losses from the absorber scale with its area and light can be concentrated to a smaller absorber and because the output powers of the TR and PV cells scale with their areas.[19,20] If the areas of the TR and PV cells are not equal, then these cannot be removed from Equation 6, and the radiation from the TR to PV cell should be described as a total power instead of as a flux. The input parameters to the model and ranges of values used in this work are summarized in Table S1.

Efficiency Limit

We now turn our attention to the efficiency limit of a solar TR-PV system. The solar conversion efficiency can be broken down into an absorber efficiency, η_{abs}, and a TR-PV

efficiency, η_{TRPV}, with $\eta = \eta_{abs}\eta_{TRPV}$. The heat-to-electricity efficiency limit of a TR converter or PV converter alone has been shown to be equal to the Carnot limit[19,40] under the following conditions: (1) the cell operates in the narrowband limit (emission to the PV cell or from the TR cell occurs only at the band-gap energy), such that sub-band-gap parasitic emission/absorption and thermal losses of the above-band-gap photons approach zero; (2) the cell operates in the radiative limit, where nonradiative generation/recombination rates approach zero; and (3) the cell voltage approaches the open-circuit voltage, where the work extracted from each photon is maximized. Applying these conditions to Equations 3 and 4 shows us that $q_{rad}(E_g)$ must approach zero, and applying this to Equation 7 yields $q_{rad}(E_g, T_a, V_{oc,TR}) = q_{rad}(E_g, T_0, V_{oc,TR})$ for an area-matched TR-PV device with aligned band gaps. Aligned band gaps are optimal because $E_{g,TR} > E_{g,PV}$ would introduce thermalization losses in the PV cell and $E_{g,TR} < E_{g,PV}$ would result in no PV power in the narrowband limit and would decrease the power density in a real system. $V_{oc,TR}$ and $V_{oc,PV}$ are the open-circuit voltages of the TR and PV cells. Simplifying, we obtain

$$\frac{E_g - eV_{oc,TR}}{T_a} = \frac{E_g - eV_{oc,PV}}{T_0} \quad \text{(Equation 9)}$$

The corresponding TR-PV efficiency is the ratio of the work extracted per photon (voltage multiplied by electron charge for each device) to the energy supplied to the TR cell per photon (band-gap energy plus potential associated with TR voltage):

$$\eta_{TRPV,lim} = \frac{-eV_{oc,TR} + eV_{oc,PV}}{-eV_{oc,TR} + E_g} \quad \text{(Equation 10)}$$

When considering Equations 9 and 10, it is important to remember that the PV voltage is positive and the TR voltage is negative. Combining and manipulating these equations provides

$$\eta_{TRPV,lim} = 1 - \frac{T_0}{T_a}, \quad \text{(Equation 11)}$$

which is the Carnot efficiency. Although unsurprising, this result is nonetheless instructive as it indicates that a solar TR-PV converter will have the same limiting efficiencies as a solar TR or solar TPV device.

To demonstrate the equivalent limiting efficiencies between solar TPVs and solar TR-PVs, we consider the case of a blackbody absorber. The limiting absorber efficiency is obtained in the absence of conductive and convective losses and is the ratio of the heat received by the TR cell to the incident solar radiation. This efficiency may be determined from Equations 1 and 2 and is

$$\eta_{abs,black} = 1 - \frac{T_a^4}{C_o f_s T_s^4} \quad \text{(Equation 12)}$$

The limiting efficiency for a TR-PV system with a blackbody absorber is therefore

$$\eta_{lim} = \left(1 - \frac{T_a^4}{C_o f_s T_s^4}\right)\left(1 - \frac{T_0}{T_a}\right) \quad \text{(Equation 13)}$$

Using Equation 13 to sweep T_a with the maximum possible concentration ($C_o = f_s^{-1} = 4.62 \times 10^4$ suns) as shown in Figure S1, one can easily find that this efficiency limit for a solar TR-PV system with a blackbody absorber is $\eta_{lim} = 85\%$ at $T_a = 2{,}544$ K. This matches the maximum efficiency of a solar TPV system.[19]

Although 85% is a very high limiting efficiency, this is not a target that can be approached in practice for several reasons. First, the maximum solar concentration

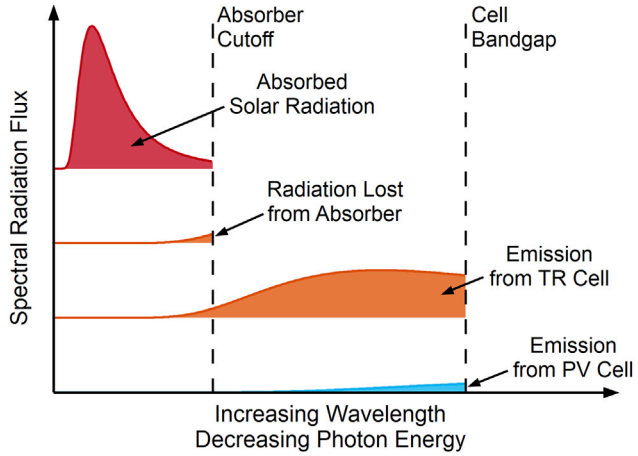

Figure 3. Schematic of Spectral Radiation Fluxes in an Ideal Solar Thermoradiative-Photovoltaic System

The red color represents solar radiation from the sun at T_s, orange represents radiation from the absorber or TR cell at T_a, and blue represents radiation from the PV cell at T_0. The cutoff energy of the absorber balances unabsorbed solar radiation with radiation lost from the absorber, and the cell band gap balances output power with loss due to excess photon energies.

and high absorber temperature are not achievable in a real system. Second, this would require an infinitely large TR area due to the narrowband emission approximation, and real cells have an optimum nonzero bandwidth.[20,48,59] Finally, nonradiative losses cannot be completely avoided in real materials.

Ideal One-Sun System

To understand the performance and potential of a solar TR-PV system, we consider a more practical idealized case: no solar concentration, an absorber area equal to the TR area, equal TR and PV band gaps, and a step-function emittance for the absorber, TR cell, and PV cell, where $\varepsilon = 1$ above the cutoff/band-gap energy and $\varepsilon = 0$ below. As described previously, a smaller absorber area than TR area may be beneficial, but there are fabrication advantages to keeping their areas equal. Matched band gaps in the TR and PV cells are optimal because these aid in spectral matching of the emission and absorption profiles between the two cells. The effects of conduction/convection losses, nonradiative losses, and optical concentration are neglected here but considered in the following sections. For this system, the spectral radiation fluxes are illustrated in Figure 3.

The absorber cutoff energy E_{abs} should balance the unabsorbed (reflected) solar radiation with the lost (emitted) thermal radiation from the absorber. Ideally, this cutoff is located at the intersection of the solar and absorber spectral radiation fluxes. A great deal of research has gone toward the development of selective solar absorbers, which can now achieve solar absorptances >95% and infrared emittances <5%.[8,60,61] Recent work on novel materials such as plasmonic nanoparticles[62] or hyperbolic metamaterials[63] have shown the potential for further improvement. The cell band gap should be low enough that substantial thermal emission is above its energy but high enough to prevent significant thermal losses of above-band-gap photons. Selective emission and absorption by semiconductor p-n diodes can be achieved by multiple strategies[13,29,30,33,35,36] as described in the introduction. Of these approaches, thin-film cells with back reflectors[13,36] are particularly promising due to their relatively simple design and potential for extremely high sub-band-gap reflectance.

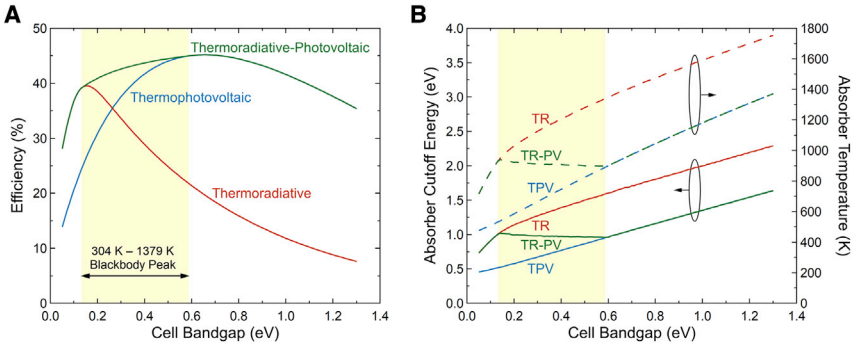

Figure 4. Performance of an Ideal One-Sun System

(A) Efficiency limits of ideal one-sun solar thermoradiative, solar thermophotovoltaic, and combined solar thermoradiative-photovoltaic devices as a function of the cell band-gap energy. The thermoradiative-photovoltaic system outperforms the other 2 devices in the highlighted region of band-gap energies, which corresponds to peak thermal emission from practically achievable temperatures.

(B) Solar absorber cutoff energies and absorber temperatures for the devices in (A).

See also Figure S2.

With these idealized inputs, we calculate the efficiency of the one-sun area-matched solar TR-PV system as a function of the cell band-gap energy and show the results in Figure 4A. For comparison, the efficiency of a solar TPV system ($V_{TR} = 0$) and of a solar TR system ($V_{PV} = 0$) are also shown. We use a Nelder-Mead simplex algorithm[64] implemented in MATLAB to find the optimum V_{TR} , V_{PV}, and E_{abs} for each band-gap energy and solve for T_a, J_{TR}, J_{PV}, and η. The corresponding absorber cutoff energies and absorber temperatures for the solar TR-PV, TPV, and TR systems are plotted in Figure 4B.

All three devices can reach impressive efficiencies of ~40%–45%, despite the use of unconcentrated light and area-matched components. Interestingly, the solar TR-PV device outperforms solar TR and solar PV systems for band gaps from 0.13 to 0.59 eV, as indicated by the shaded yellow region in Figures 4A and 4B. This range of band gaps is particularly important for solar-thermal energy conversion because lower band gaps enable higher power densities[59] and allow for a lower temperature absorber. The former advantage of low band gaps results from having more radiation exchange above the band gap for a given hot-side temperature, and the latter advantage of low band gaps is evident from the absorber temperatures in Figure 4B; in the region where TR-PVs outperform the other devices, the optimum absorber temperature is relatively constant at ~920 K. This is much lower than the typical solar TPV emitter temperatures used with higher band gap cells,[14,27,28,31] which provides substantial engineering and design advantages. Importantly, the efficiency improvements of the TR-PV device over a broad range of low band gaps could enable the use of a variety of low-band-gap materials that are avoided in solar TPV systems due to their efficiency drop-off in Figure 4A. We also see from Figure 4B that in this region, the ideal TR-PV device has absorber temperatures and absorber cutoff energies between those of the solar TR and solar TPV devices. This arises from negative luminescent effects on the radiation exchange. As indicated by Equation 5, the negative TR voltage reduces above-band-gap emission, leading to a higher absorber temperature and higher optimum absorber cutoff energy to reduce absorber emission losses. From 0.13 to 0.59 eV, V_{TR} is smaller in magnitude for the TR-PV device than it is for the TR device, causing the intermediate values of E_{abs} and T_a.

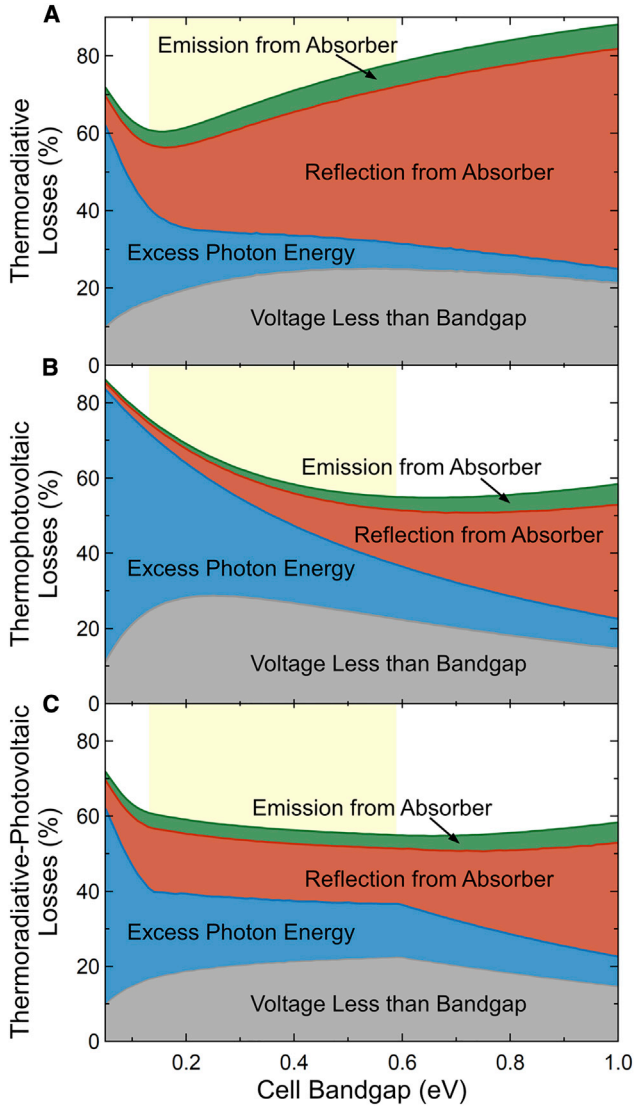

Figure 5. Losses in an Ideal One-Sun System

Losses in ideal one-sun (A) solar thermoradiative, (B) solar thermophotovoltaic, and (C) solar thermoradiative-photovoltaic systems corresponding to the devices in Figure 4. The thermoradiative-photovoltaic system outperforms single devices by optimizing the tradeoff between excess photon energy losses and reflection losses.
See also Figure S2.

The reasons for improved TR-PV performance compared to the other devices are best understood by comparing the different loss mechanisms. For this idealized case, the four losses are emission from the absorber, reflection of solar radiation from the absorber, photon energy exchange between the TR and PV cells in excess of the band-gap energy, and intrinsic losses due to operational voltages less than the band gap. These losses are depicted for the TR, TPV, and TR-PV devices in Figures 5A–5C, respectively. For all three systems, emission from the absorber is a fairly small loss mechanism. More significant are reflection from the absorber and excess photon energy losses. Reflection losses are higher for the TR device in Figure 5A than for the TPV device in Figure 5B because the negative TR voltage suppresses its thermal emission. This leads to a higher absorber temperature and higher optimal

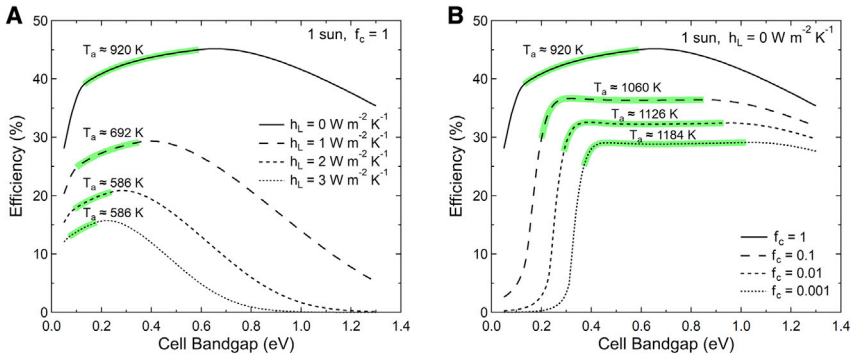

Figure 6. Effects of Non-idealities on System Performance

Effects of (A) conductive/convective heat losses from the solar absorber and (B) nonradiative losses on efficiency. The highlighted regions indicate where a solar thermoradiative-photovoltaic device outperforms a solar thermoradiative or solar thermophotovoltaic system alone, and the average (approximately constant) absorber temperature is listed for each of these regions.
See also Figures S3 and S4.

absorber cutoff energy (see Figure 4B). However, excess photon energy losses are lower for the TR device in Figure 5A than for the TPV device in Figure 5B for a similar reason; the negative TR voltage suppresses the thermal emission of photons far above the band gap. From 0.13 to 0.59 eV, the TR-PV device can balance these two loss mechanisms by using both a TR cell and a PV cell. The voltages of each (see Figure S2) and absorber cutoff energy can be optimized to reduce the high reflection losses of a TR system while also reducing the high excess photon energy losses of a TPV system, as shown by Figure 5C. This ability to balance losses also helps the TR-PV device to be relatively insensitive to band gap between the TR and TPV peak efficiencies. Below this band-gap range, the ideal solar TR-PV converter acts only as a solar TR converter (V_{PV} = 0), and above this band-gap range, the solar TR-PV converter acts only as a solar TPV converter (V_{TR} = 0).

Effects of Non-idealities

Because real devices cannot avoid conduction, convection, and nonradiative losses, it is important to investigate how these affect system efficiency. Conduction/convection losses are included with a nonzero loss coefficient h_L, as shown in Figure 2. Nonradiative losses are counted by setting the radiative fraction of generation/recombination f_c to values <1, as described earlier. The effects of conduction/convection losses and nonradiative losses on solar TR-PV efficiency are plotted in Figures 6A and 6B, respectively. The green-highlighted regions of the curves in each plot indicate the band gaps for which a solar TR-PV system outperforms a solar TR or solar TPV converter alone, and the temperatures listed indicate the average absorber/TR temperature for these regions, which is approximately constant. The detailed absorber cutoff energies, absorber temperatures, and operating voltages of these devices are plotted in Figures S3 and S4.

Unsurprisingly, conduction/convection losses from the absorber in Figure 6A tend to decrease solar TR-PV performance. With additional heat losses, the lower absorber temperatures of solar TPV converters lead to reduced efficiency at high band gaps and a solar TPV efficiency peak at lower band gaps, as seen in Figure 6A. This causes the green-highlighted region to shift to lower band gaps as heat losses increase. Because these have a large impact on the efficiency of one-sun TR-PV systems, it is crucial to minimize heat losses in practical systems. A different method to reduce their impact is to operate under optical concentration, which is examined in the

following section. Nonradiative losses in Figure 6B also decrease efficiency as expected, but the TR-PV performance is surprisingly robust in the presence of these losses, even when f_c is very small. Below a band gap of 0.5 eV, for instance, an f_c value of 0.001 yields large nonradiative loss rates between 10^{25} and 10^{29} cm^{-3} s^{-1} in the TR cell and between 10^{21} and 10^{23} cm^{-3} s^{-1} in the PV cell, but the solar conversion efficiency still reaches ~29%. This results from the fact that solar TR-PV devices operate at lower magnitude V_{TR} and V_{PV} than TR or TPV converters alone, as shown in Figures S3 and S4, and nonradiative losses tend to have an exponential dependence on cell voltage.[54] The combined system is also more tolerant to nonradiative losses in the TR cell, because no energy is lost to the surroundings when there is a nonradiative generation event. When this occurs, the TR cell current is reduced, but the PV cell can still use the energy of the emitted photon. As a result of the ability of the TR-PV system to retain energy with nonradiative generation in the TR cell, the combined system outperforms the other devices over a larger band-gap range when nonradiative losses are considered. This large band-gap range where TR-PV devices achieve higher efficiency than TPV or TR devices alone further highlights the possibility of using a variety of low band-gap materials with solar TR-PV systems for efficient solar thermal energy conversion.

Combined Losses with Optical Concentration

Although examining different loss mechanisms on their own is instructive to understand how they affect performance, it is clear from some of the differing trends in Figure 6 that their interaction will be significant. In addition, operating these devices under optical concentration could allow smaller devices to be made at a lower cost. We therefore consider a solar TR-PV system with combined losses under varying optical concentration selected to be representative of an attainable system.

For the absorber, we model conductive/convective losses with a loss coefficient of h_L = 1 W m^{-2} K^{-1}, which is a reasonable assumption for evacuated absorbers[8] and is beginning to be approached for non-evacuated absorbers coated with insulating transparent aerogels.[65,66] Nonideal optical properties are included by setting $\varepsilon_a(E)$ = 0.98 above E_{abs} and $\varepsilon_a(E)$ = 0.02 below E_{abs}, which is similar to materials currently available[8,60,61] and is being demonstrated with novel materials for high solar absorptance,[62,63] as discussed earlier. We choose an absorber cutoff energy of 1 eV based on the results discussed previously. Instead of modeling the incident solar energy as light from a blackbody, we use the AM 1.5 D spectrum[67] multiplied by C_o for optical concentration.

For the TR and PV cells, we choose cell band gaps of 0.35 eV, which is in the range in which solar TR-PV converters are expected to outperform the other devices. This is also near the efficiency peaks observed in Figures 6A and 6B when different loss mechanisms are included. Furthermore, this band gap is low enough to have substantial thermal radiation above its band gap and be spectrally well matched to relatively low absorber temperatures. Finally, this band gap is achievable by the epitaxial growth of the InGaAsSb material system.[68–70] Nonradiative generation/recombination is included in the cells by setting f_c = 0.01. Nonideal optical properties of the cells are included by setting $\varepsilon_{TR}(E)$ and $\varepsilon_{PV}(E)$ to 0.95 above E_g and 0.02 below E_g, which can be achieved by thin-film cells with a good back reflector and front anti-reflectance coating.[13,36,37] We continue to neglect any temperature dependence of material and optical properties of the absorber and cells.

With these parameters, we plot the solar TR-PV efficiency in Figure 7A and the associated loss mechanisms in Figure 7B as a function of optical concentration. For

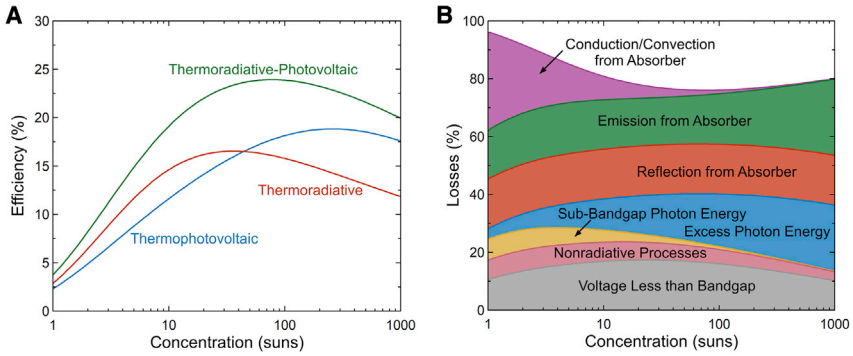

Figure 7. Performance of a System with Combined Loss Mechanisms under Optical Concentration

(A) Efficiency of 0.35 eV band-gap solar thermoradiative, solar thermophotovoltaic, and solar thermoradiative-photovoltaic systems with heat losses h_L = 1 W m^{-2} K^{-1}, nonradiative losses f_c = 0.01, and nonideal optical properties for varying solar concentration.

(B) Losses for the thermoradiative-photovoltaic system in (A). The remaining white region above the losses represents the useful output power.

See also Figure S5.

comparison, the efficiency of a solar TPV and solar TR converter with the same inputs is also shown in Figure 7A. The absorber temperatures and operating voltages for these devices are shown in Figure S5. The solar TR-PV system outperforms the TR and TPV devices for all concentration ratios and achieves a maximum efficiency of ~24% at 80 suns. This is 1.27 times higher than the maximum TPV efficiency and 1.45 times higher than the maximum TR efficiency, representing a substantial performance improvement over the other devices. At lower concentrations, its performance improvement over TPV systems is even more pronounced, reaching up to a 7.9% absolute efficiency gain at 18 suns. It is also worth noting that the peak TR-PV efficiency is similar to that of commercial concentrating solar power plants,[8] and the relatively low concentration of the efficiency peak means that solar TR-PV systems could serve as heat engines for low-cost single-axis tracking systems. In addition, this TR-PV converter could likely be optimized to further boost its efficiency, and it could be coupled to a thermal storage system for continuous electricity generation.

If instead of fixing the band gap at 0.35 eV we vary the band gap for several concentrations, we find that solar TR-PV converters still outperform solar TR and solar TPV converters for low concentrations, as shown in Figure S6. For a higher concentration of 100 suns (Figures S6C and S6F), solar TPVs can achieve slightly higher efficiencies, but they require higher band gaps >0.6 eV. An important reason that solar TR-PVs perform better than the other devices in this more realistic system is the nonideal optical properties of the cells. As the sub-band-gap emittance is increased above zero, parasitic radiation exchange below the band gap also increases. Nonideal optical properties therefore cause lower band-gap materials to be favored to decrease these losses and improve the spectral efficiency (photon utilization)[15] of the converter. This effect can be seen by comparing Figures S6A–S6C, which have the same sub-band-gap emittance of 0.02, to Figures S6D–S6F, which have an increased sub-band-gap emittance of 0.10. The poorer spectral selectivity of the latter case results in larger relative performance gains of TR-PVs compared to TPVs.

The reasons for an optimum concentration of 80 suns with the 0.35 eV TR-PV system can be understood by examining the losses in Figure 7B. Conduction/convection from the absorber accounts for a large portion of losses at low concentration as

expected from the one-sun results in Figure 6A. These losses scale with T_a, but the power produced scales with T_a^4, making heat losses less significant as concentration increases and causing the efficiency to rise. As concentration increases further and T_a passes ~1,400 K (see Figure S5A), thermal emission from the absorber and thermal losses of far above-band-gap photons begin to dominate, and the efficiency decreases. We emphasize that the peak efficiency value and the concentration at which it is reached are specific to the combination of losses, band gap, and absorber cutoff energy selected for this system. These could be tuned to design for a particular concentration ratio, a specific band gap, or other system parameters.

The breakdown of losses in Figure 7B can also provide some insight and guidance to further improve solar TR-PV performance. With nonideal optical properties, parasitic sub-band-gap absorption and emission occurs between the TR and PV cells. This decreases at higher concentration when the absorber temperature rises because more thermal radiation occurs above the band gap. With improved cell spectral selectivity, this loss can be substantially reduced at low concentrations. Emission and reflection losses from the absorber also result in part from nonideal optical components, but these are less sensitive to concentration. Improved spectral selectivity here would reduce these losses across a broad range of concentration ratios. Conduction/convection losses from the absorber display the most drastic dependence on concentration and are most substantial at concentrations <10 suns. To enable very-low-concentration and low-temperature solar TR-PV systems, conduction/convection losses must be very low. Finally, we note that increasing the ratio of the TR area to the absorber area could have a substantial impact on these losses and the resulting device efficiency. This could be a promising strategy to minimize conduction, convection, and emission losses from the absorber. We would expect the performance advantages of solar TR-PV cells to extend to these system configurations as well.

DISCUSSION

Solar TR-PV systems display clear performance benefits compared to solar TR or solar TPV systems, which results from their ability to use the advantages of each device. These performance enhancements occur at low to moderate band gaps in an ideal range for solar-thermal energy harvesting. Similar to a solar TPV or solar TR device, heat losses and nonradiative losses degrade performance, but TR-PV systems can still achieve high efficiencies and outperform individual devices when these are considered. A model of a 0.35-eV band gap solar TR-PV system with combined loss mechanisms shows that they can substantially outperform solar TPV and solar TR converters at low optical concentrations. Importantly, solar TR-PV converters can be paired with thermal storage to provide reliable electricity generation, even with intermittent sunlight.

A solar TR-PV device is necessarily more complex than a solar PV, a solar TPV, or a solar TR converter. This will lead to a higher cost on a per-cell-area basis than the other devices, which motivates TR-PV use when it can achieve substantially higher efficiencies than the other uncombined devices. For example, the TR-PV system examined in Figure 7 displays the most significant efficiency gains compared to both a solar TR or a solar TPV system at a concentration of ~45 suns. This would be a good operational target for this particular TR-PV device, as it could achieve lower cost per unit power for this concentration. Low levels of concentration such as 45 suns are also not typically targeted for solar TPV energy conversion because TPVs favor higher temperature emitters and higher band gaps, as shown in Figure 4.

A TR-PV system could therefore enable efficient solar energy conversion for low concentration or in conjunction with hybrid PV-thermal systems,[71] which reduces the need for costly high-performance tracking, optics, and cooling accessories.

Although this preliminary analysis of solar TR-PV systems is encouraging, additional research is needed to model and test their operation in greater detail. In particular, the effect of TR temperature on nonradiative losses could be significant, depending on the TR material.[48,72] Auger losses can increase significantly as temperature increases, which may require the use of strategies for Auger suppression such as the use of a p-i-n diode to reduce carrier concentrations in the active region,[73,74] interface-induced Auger suppression in type II and type III heterostructures,[75–77] or careful engineering of the confinement potential in nanostructure-based devices.[78] The band gap of a device also generally shifts with temperature, which could require different material compositions of the TR and PV cells to align their band gaps. Maintaining stability and good spectral selectivity of the solar absorber at elevated temperatures may also be a challenge,[79] but there are several examples of good progress on this front.[8] Other more practical considerations include investigating the effects of heat losses at the edges of the devices and studying large TR:absorber area ratios, which could boost performance beyond what has been shown here. Nevertheless, this promising initial performance comparison suggests that solar TR-PV systems could be a path to efficient and low-cost solar-thermal energy conversion.

EXPERIMENTAL PROCEDURES

Resource Availability

Lead Contact

Further information and requests for resources should be directed to and will be fulfilled by the Lead Contact, Eric Tervo (eric.tervo@nrel.gov).

Materials Availability

This study did not generate new unique reagents.

Data and Code Availability

This study did not generate new algorithms. The published article includes all of the methods used to produce the results.

SUPPLEMENTAL INFORMATION

Supplemental Information can be found online at https://doi.org/10.1016/j.xcrp.2020.100258.

ACKNOWLEDGMENTS

The authors would like to thank Dr. Andreas Pusch of the University of New South Wales for helpful discussions. This work was authored by the National Renewable Energy Laboratory (NREL), operated by the Alliance for Sustainable Energy, LLC, for the US Department of Energy (DOE) under contract no. DE-AC36-08GO28308. This work was supported by the Laboratory Directed Research and Development (LDRD) Program at NREL. The views expressed in the article do not necessarily represent the views of the DOE or the US government.

AUTHOR CONTRIBUTIONS

Conceptualization, Methodology, & Writing – Original Draft, E.J.T.; Investigation & Writing – Review & Editing: E.J.T., W.A.C., E.S.T., M.A.S., and A.J.F.

DECLARATION OF INTERESTS

The authors declare no competing interests.

Received: September 1, 2020
Revised: October 19, 2020
Accepted: October 27, 2020
Published: November 25, 2020

REFERENCES

1. Bauer, T., Steinmann, W.-D., Laing, D., and Tamme, R. (2012). Thermal Energy Storage Materials and Systems. Annu. Rev. Heat Transfer *15*, 131–177.

2. Liu, M., Steven Tay, N.H., Bell, S., Belusko, M., Jacob, R., Will, G., Saman, W., and Bruno, F. (2016). Review on concentrating solar power plants and new developments in high temperature thermal energy storage technologies. Renew. Sustain. Energy Rev. *53*, 1411–1432.

3. Pelay, U., Luo, L., Fan, Y., Stitou, D., and Rood, M. (2017). Thermal energy storage systems for concentrated solar power plants. Renew. Sustain. Energy Rev. *79*, 82–100.

4. Alva, G., Lin, Y., and Fang, G. (2018). An overview of thermal energy storage systems. Energy *144*, 341–378.

5. Kashyap, V., Sakunkaewkasem, S., Jafari, P., Nazari, M., Eslami, B., Nazifi, S., Irajizad, P., Marquez, M.D., Lee, T.R., and Ghasemi, H. (2019). Full Spectrum Solar Thermal Energy Harvesting and Storage by a Molecular and Phase-Change Hybrid Material. Joule *3*, 3100–3111.

6. Schmidt, O., Hawkes, A., Gambhir, A., and Staffell, I. (2017). The future cost of electrical energy storage based on experience rates. Nat. Energy *2*, 17110.

7. Amy, C., Seyf, H.R., Steiner, M.A., Friedman, D.J., and Henry, A. (2019). Thermal energy grid storage using multi-junction photovoltaics. Energy Environ. Sci. *12*, 334–343.

8. Weinstein, L.A., Loomis, J., Bhatia, B., Bierman, D.M., Wang, E.N., and Chen, G. (2015). Concentrating Solar Power. Chem. Rev. *115*, 12797–12838.

9. Romero, M., and Steinfeld, A. (2012). Concentrating solar thermal power and thermochemical fuels. Energy Environ. Sci. *5*, 9234–9245.

10. Kraemer, D., Jie, Q., McEnaney, K., Cao, F., Liu, W., Weinstein, L.A., Loomis, J., Ren, Z., and Chen, G. (2016). Concentrating solar thermoelectric generators with a peak efficiency of 7.4%. Nat. Energy *1*, 16153.

11. Wang, Y., Liu, H., and Zhu, J. (2019). Solar thermophotovoltaics: Progress, challenges, and opportunities. APL Mater. *7*, 080906.

12. Chan, W.R., Stelmakh, V., Ghebrebrhan, M., Soljačić, M., Joannopoulos, J.D., and Čelanović, I. (2017). Enabling efficient heat-to-electricity generation at the mesoscale. Energy Environ. Sci. *10*, 1367–1371.

13. Omair, Z., Scranton, G., Pazos-Outón, L.M., Xiao, T.P., Steiner, M.A., Ganapati, V., Peterson, P.F., Holzrichter, J., Atwater, H., and Yablonovitch, E. (2019). Ultraefficient thermophotovoltaic power conversion by band-edge spectral filtering. Proc. Natl. Acad. Sci. USA *116*, 15356.

14. Bhatt, R., Kravchenko, I., and Gupta, M. (2020). High-efficiency solar thermophotovoltaic system using a nanostructure-based selective emitter. Sol. Energy *197*, 538–545.

15. Burger, T., Sempere, C., Roy-Layinde, B., and Lenert, A. (2020). Present Efficiencies and Future Opportunities in Thermophotovoltaics. Joule *4*, 1660–1680.

16. Nelson, R.E. (2003). A brief history of thermophotovoltaic development. Semicond. Sci. Technol. *18*, S141–S143.

17. Bauer, T. (2011). Thermophotovoltaics: Basic Principles and Critical Aspects of System Design (Springer-Verlag).

18. Zhou, Z., Enas, S., Sun, Y., and Bermel, P. (2016). Solar thermophotovoltaics: reshaping the solar spectrum. Nanophotonics *5*, 1–21.

19. Harder, N.-P., and Wurfel, P. (2003). Theoretical limits of thermophotovoltaic solar energy conversion. Semicond. Sci. Technol. *18*, S151–S157.

20. Rephaeli, E., and Fan, S. (2009). Absorber and emitter for solar thermo-photovoltaic systems to achieve efficiency exceeding the Shockley-Queisser limit. Opt. Express *17*, 15145–15159.

21. Datas, A., and Algora, C. (2013). Global optimization of solar thermophotovoltaic systems. Prog. Photovolt. Res. Appl. *21*, 1040–1055.

22. Nam, Y., Yeng, Y.X., Lenert, A., Bermel, P., Celanovic, I., Soljačić, M., and Wang, E.N. (2014). Solar thermophotovoltaic energy conversion systems with two-dimensional tantalum photonic crystal absorbers and emitters. Sol. Energy Mater. Sol. Cells *122*, 287–296.

23. Wang, H., Chang, J.-Y., Yang, Y., and Wang, L. (2016). Performance analysis of solar thermophotovoltaic conversion enhanced by selective metamaterial absorbers and emitters. Int. J. Heat Mass Transf. *98*, 788–798.

24. Jiang, D., and Yang, W. (2017). A dielectric-encapsulated 2D photonic crystal based solar thermophotovoltaic power generator. Appl. Therm. Eng. *125*, 1253–1259.

25. Chang, C.-C., Kort-Kamp, W.J.M., Nogan, J., Luk, T.S., Azad, A.K., Taylor, A.J., Dalvit, D.A.R., Sykora, M., and Chen, H.-T. (2018). High-Temperature Refractory Metasurfaces for Solar Thermophotovoltaic Energy Harvesting. Nano Lett. *18*, 7665–7673.

26. Ni, Q., McBurney, R., Alshehri, H., and Wang, L. (2019). Theoretical analysis of solar thermophotovoltaic energy conversion with selective metafilm and cavity reflector. Sol. Energy *191*, 623–628.

27. Lenert, A., Bierman, D.M., Nam, Y., Chan, W.R., Celanović, I., Soljačić, M., and Wang, E.N. (2014). A nanophotonic solar thermophotovoltaic device. Nat. Nanotechnol. *9*, 126–130.

28. Ungaro, C., Gray, S.K., and Gupta, M.C. (2015). Solar thermophotovoltaic system using nanostructures. Opt. Express *23*, A1149–A1156.

29. Makoto, S., Asaka, K., and Hiroo, Y. (2015). High-efficiency solar-thermophotovoltaic system equipped with a monolithic planar selective absorber/emitter. J. Photonics Energy *5*, 1–9.

30. Bierman, D.M., Lenert, A., Chan, W.R., Bhatia, B., Celanović, I., Soljačić, M., and Wang, E.N. (2016). Enhanced photovoltaic energy conversion using thermally based spectral shaping. Nat. Energy *1*, 16068.

31. Kohiyama, A., Shimizu, M., and Yugami, H. (2016). Unidirectional radiative heat transfer with a spectrally selective planar absorber/emitter for high-efficiency solar thermophotovoltaic systems. Appl. Phys. Express *9*, 112302.

32. Seyf, H.R., and Henry, A. (2016). Thermophotovoltaics: a potential pathway to high efficiency concentrated solar power. Energy Environ. Sci. *9*, 2654–2665.

33. Chan, W.R., Bermel, P., Pilawa-Podgurski, R.C.N., Marton, C.H., Jensen, K.F., Senkevich, J.J., Joannopoulos, J.D., Soljačić, M., and Celanovic, I. (2013). Toward high-energy-density, high-efficiency, and moderate-temperature chip-scale thermophotovoltaics. Proc. Natl. Acad. Sci. USA *110*, 5309.

34. Fan, S. (2017). Thermal Photonics and Energy Applications. Joule *1*, 264–273.

35. Wernsman, B., Siergiej, R.R., Link, S.D., Mahorter, R.G., Palmisiano, M.N., Wehrer, R.J., Schultz, R.W., Schmuck, G.P., Messham, R.L., Murray, S., et al. (2004). Greater than 20% radiant heat conversion efficiency of a thermophotovoltaic radiator/module system using reflective spectral control. IEEE Trans. Electron Dev. *51*, 512–515.

36. Burger, T., Fan, D., Lee, K., Forrest, S.R., and Lenert, A. (2018). Thin-Film Architectures with High Spectral Selectivity for Thermophotovoltaic Cells. ACS Photonics *5*, 2748–2754.

37. Fan, D., Burger, T., McSherry, S., Lee, B., Lenert, A., and Forrest, S.R. (2020). Near-perfect photon utilization in an air-bridge thermophotovoltaic cell. Nature *586*, 237–241.

38. Byrnes, S.J., Blanchard, R., and Capasso, F. (2014). Harvesting renewable energy from Earth's mid-infrared emissions. Proc. Natl. Acad. Sci. USA *111*, 3927.

39. Strandberg, R. (2015). Theoretical efficiency limits for thermoradiative energy conversion. J. Appl. Physiol. *117*, 055105.

40. Santhanam, P., and Fan, S. (2016). Thermal-to-electrical energy conversion by diodes under negative illumination. Phys. Rev. B *93*, 161410.

41. Ono, M., Santhanam, P., Li, W., Zhao, B., and Fan, S. (2019). Experimental demonstration of energy harvesting from the sky using the negative illumination effect of a semiconductor photodiode. Appl. Phys. Lett. *114*, 161102.

42. Wang, J., Chen, C.-H., Bonner, R., and Anderson, W.G. (2019). Thermo-Radiative Cell - A New Waste Heat Recovery Technology for Space Power Applications. https://doi.org/10.2514/6.2019-3977.

43. Hsu, W.-C., Tong, J.K., Liao, B., Huang, Y., Boriskina, S.V., and Chen, G. (2016). Entropic and Near-Field Improvements of Thermoradiative Cells. Sci. Rep. *6*, 34837.

44. Lin, C., Wang, B., Teo, K.H., and Zhang, Z. (2017). Performance comparison between photovoltaic and thermoradiative devices. J. Appl. Physiol. *122*, 243103.

45. Zhang, X., Peng, W., Lin, J., Chen, X., and Chen, J. (2017). Parametric design criteria of an updated thermoradiative cell operating at optimal states. J. Appl. Physiol. *122*, 174505.

46. Buddhiraju, S., Santhanam, P., and Fan, S. (2018). Thermodynamic limits of energy harvesting from outgoing thermal radiation. Proc. Natl. Acad. Sci. USA *115*, E3609.

47. Tervo, E., Bagherisereshki, E., and Zhang, Z. (2018). Near-field radiative thermoelectric energy converters: a review. Front. Energy *12*, 5–21.

48. Pusch, A., Gordon, J.M., Mellor, A., Krich, J.J., and Ekins-Daukes, N.J. (2019). Fundamental Efficiency Bounds for the Conversion of a Radiative Heat Engine's Own Emission into Work. Phys. Rev. Appl. *12*, 064018.

49. García, G., Fernández, J.J., Palacios, P., and Wahnón, P. (2019). Thermoradiative Cells Based on a p-type Cu3SbSe4 Semiconductor: Application of a Detailed Balance Model. J. Electron. Mater. *48*, 6777–6785.

50. Zhang, X., Ang, Y.S., Chen, J.c., and Ang, L.K. (2019). Design of an InSb thermoradiative system for harvesting low-grade waste heat. Opt. Lett. *44*, 3354–3357.

51. Liao, T., Zhang, X., Chen, X., Lin, B., and Chen, J. (2017). Negative illumination thermoradiative solar cell. Opt. Lett. *42*, 3236–3238.

52. Liao, T., Yang, Z., Chen, X., and Chen, J. (2019). Thermoradiative–Photovoltaic Cells. IEEE Trans. Electron Dev. *66*, 1386–1389.

53. Rühle, S. (2016). Tabulated values of the Shockley–Queisser limit for single junction solar cells. Sol. Energy *130*, 139–147.

54. Shockley, W., and Queisser, H.J. (1961). Detailed Balance Limit of Efficiency of p-n Junction Solar Cells. J. Appl. Physiol. *32*, 510–519.

55. Brennan, K.F. (1999). The Physics of Semiconductors: With Applications to Optoelectronic Devices (Cambridge University Press).

56. Wurfel, P. (1982). The chemical potential of radiation. J. Phys. C Solid State Phys. *15*, 3967–3985.

57. Landsberg, P.T. (1981). Photons at non-zero chemical potential. J. Phys. C Solid State Phys. *14*, L1025–L1027.

58. Nellis, G., and Klein, S.A. (2009). Heat Transfer (Cambridge University Press).

59. Baldasaro, P.F., Raynolds, J.E., Charache, G.W., DePoy, D.M., Ballinger, C.T., Donovan, T., and Borrego, J.M. (2001). Thermodynamic analysis of thermophotovoltaic efficiency and power density tradeoffs. J. Appl. Physiol. *89*, 3319–3327.

60. Bermel, P., Lee, J., Joannopoulos, J.D., Celanovic, I., and Soljačić, M. (2012). Selective solar absorbers. Annu. Rev. Heat Transfer *15*, 231–254.

61. Cao, F., McEnaney, K., Chen, G., and Ren, Z. (2014). A review of cermet-based spectrally selective solar absorbers. Energy Environ. Sci. *7*, 1615–1627.

62. Zhou, L., Tan, Y., Ji, D., Zhu, B., Zhang, P., Xu, J., Gan, Q., Yu, Z., and Zhu, J. (2016). Self-assembly of highly efficient, broadband plasmonic absorbers for solar steam generation. Sci. Adv. *2*, e1501227.

63. Wang, Z., Zhang, Z.M., Quan, X., and Cheng, P. (2018). A perfect absorber design using a natural hyperbolic material for harvesting solar energy. Sol. Energy *159*, 329–336.

64. Lagarias, J.C., Reeds, J.A., Wright, M.H., and Wright, P.E. (1998). Convergence Properties of the Nelder–Mead Simplex Method in Low Dimensions. SIAM J. Optim. *9*, 112–147.

65. Zhao, L., Bhatia, B., Yang, S., Strobach, E., Weinstein, L.A., Cooper, T.A., Chen, G., and Wang, E.N. (2019). Harnessing Heat Beyond 200 °C from Unconcentrated Sunlight with Nonevacuated Transparent Aerogels. ACS Nano *13*, 7508–7516.

66. Strobach, E., Bhatia, B., Yang, S., Zhao, L., and Wang, E.N. (2019). High temperature stability of transparent silica aerogels for solar thermal applications. APL Mater. *7*, 081104.

67. ASTM International (2012). ASTM G173-03(2012), Standard Tables for Reference Solar Spectral Irradiances: Direct Normal and Hemispherical on 37° Tilted Surface. https://www.astm.org/Standards/G173.htm.

68. Cherng, M.J., Jen, H.R., Larsen, C.A., Strigfellow, G.B., Lundt, H., and Taylor, P.C. (1986). MOVPE growth of GaInAsSb. J. Cryst. Growth *77*, 408–417.

69. Wang, C.A., Choi, H.K., Ransom, S.L., Charache, G.W., Danielson, L.R., and DePoy, D.M. (1999). High-quantum-efficiency 0.5 eV GaInAsSb/GaSb thermophotovoltaic devices. Appl. Phys. Lett. *75*, 1305–1307.

70. Rogers, V., Deitz, J.I., Blumer, A.N., Carlin, J.A., Grassman, T.J., and Krishna, S. (2020). InAs1−ySby virtual substrates grown by MOCVD for long wave infrared detectors. J. Cryst. Growth *535*, 125552.

71. Weinstein, L.A., McEnaney, K., Strobach, E., Yang, S., Bhatia, B., Zhao, L., Huang, Y., Loomis, J., Cao, F., Boriskina, S.V., et al. (2018). A Hybrid Electric and Thermal Solar Receiver. Joule *2*, 962–975.

72. Ekins-Daukes, N.J.K., Al, L., Nielsen, M.P., Mellor, A.V., and Pusch, A. (2020). Generating power at night using a thermoradiative diode, how is this possible? In Proceedings of the IEEE 47th Photovoltaics Specialists Conference, Virtual.

73. White, A.M. (1986). Auger suppression and negative resistance in low gap PIN diode structures. Infrared Phys. *26*, 317–324.

74. Nash, G.R., Ashby, M.K., Lindle, J.R., Gordon, N.T., Bewley, W.W., Meyer, J.R., Giess, J., Haworth, L., and Ashley, T. (2003). Long wavelength infrared negative luminescent devices with strong Auger suppression. J. Appl. Physiol. *94*, 7300–7304.

75. Zegrya, G.G., and Andreev, A.D. (1995). Mechanism of suppression of Auger recombination processes in type-II heterostructures. Appl. Phys. Lett. *67*, 2681–2683.

76. Mohseni, H., Litvinov, V.I., and Razeghi, M. (1998). Interface-induced suppression of the Auger recombination in type-II InAs/GaSb superlattices. Phys. Rev. B Condens. Matter Mater. Phys. *58*, 15378–15380.

77. Slonopas, A., and Tomkinson, D. (2017). Study of the Natural Auger Suppression Mechanism in Heterostructures through Heteroboundary Engineering. J. Phys. Chem. A *121*, 7745–7750.

78. Cragg, G.E., and Efros, A.L. (2010). Suppression of Auger Processes in Confined Structures. Nano Lett. *10*, 313–317.

79. Cao, F., Kraemer, D., Tang, L., Li, Y., Litvinchuk, A.P., Bao, J., Chen, G., and Ren, Z. (2015). A high-performance spectrally-selective solar absorber based on a yttria-stabilized zirconia cermet with high-temperature stability. Energy Environ. Sci. *8*, 3040–3048.